AIMS Materials Science, 12(4): 877–892.
DOI: 10.3934/matersci.2025038
Received: 02 July 2025
Revised: 19 August 2025
Accepted: 22 August 2025
Published: 01 September 2025

https://www.aimspress.com/journal/Materials

Research article

Study on photocatalytic activity of ZnO-Zn_2TiO_4 for the ceramic glaze

Weida Hu[1,2,3,*], Jiaming Lin[1,2], Qi Xu[1,2], Tong Yu[2], Jingxiong Liu[1,2], Zhiquan Xiao[1], Hong Wang[3] and Qijian Li[3]

[1] School of Materials Science and Engineering, Hunan University of Technology, Zhuzhou, 412007, China
[2] Liling Ceramic College, Hunan University of Technology, Zhuzhou, 412007, China
[3] Hunan Yangdong Porcelain Insulators & Electric Co. Ltd, The Ultra High Voltage Insulation Materials of Hunan Engineering Technology Research Center, Zhuzhou, 412205, China

* **Correspondence:** Email: 203huweida@163.com; Tel: +86-189-7533-4250.

Abstract: Due to the high sintering temperature of traditional ceramics, most photocatalytic substances in the ceramic glaze will lose efficacy. In this study, the photocatalyst of ZnO-Zn_2TiO_4 were synthesized by the sol-hydrothermal method and sintered at 1300 ℃. The photocatalytic activity of ZnO-Zn_2TiO_4 was tested by the degradation of methylene blue (MB) under sunlight irradiation at room temperature. Then, selecting the best catalytic effect of ZnO-Zn_2TiO_4 was mixed with the ceramic glaze and sintered at 1300 ℃, which was also tested by the degradation of MB. The results showed that when the ZnO-Zn_2TiO_4 was the molar ratio of Ti:Zn = 1:8 and added into the ceramic glaze with 15% mass percentage after sintering 1300 ℃, it exhibited superior photocatalytic efficiency in degrading MB. This study presents a novel approach for preparing high-temperature (1300 ℃) glazes with enhanced photocatalytic properties.

Keywords: photocatalysis; high temperature; ZnO; Zn_2TiO_4; ceramic glaze

1. Introduction

With the rapid advancement of science and technology, the utilization of anti-pollution materials assumes a pivotal role. In the context of traditional ceramic industry, this is primarily manifested in the incorporation of antibacterial and self-cleaning properties into ceramic glazes. However, it is worth

noting that photocatalysis technology now offers an exceptional solution for decontaminating ceramic glazes [1–3].

Most of the photocatalysts employed are metal oxides or sulfides, such as TiO_2, ZnO, CdS, WO_3, and SnO_2 [4–6]. Alternatively, photocatalysts can be fabricated by coupling two semiconductors; for example, TiO_2-CdS, TiO_2-SnO_2, TiO_2-WO_3, and TiO_2-ZnO [7–10]. To enhance the photocatalytic performance of ceramic glaze, two primary approaches can be employed. Initially, applying a semiconductor thin film with photocatalytic activity onto the surface of the glaze; however, this method often leads to weak bonding between the film and the glaze, making it susceptible to scratching and subsequently reducing its photocatalytic effectiveness. Alternatively, the photocatalysts are incorporated into the ceramic glaze mixture followed by sintering [11–14]. Although this method effectively addresses the limitations of the weak combination between the photocatalytic film and the ceramic glaze, it is essential to ensure a sintering temperature below 1000 ℃ due to potential degradation of photocatalytic properties at elevated temperatures.

There is limited research on investigating the photocatalytic properties of high-temperature prepared ceramic glazes. For instance, by incorporating modified TiO_2 into the ceramic glaze, the transition temperature from anatase to rutile could be extended from 700 to 900 ℃, thereby enhancing the photocatalytic activity of TiO_2 on the ceramic glaze at higher temperatures [15]. He [16] prepared a SiO_2-TiO_2 composite oxide by incorporating TiO_2 into SiO_2 to retard the formation of rutile, resulting in enhanced high temperature stability and photocatalytic properties. However, when used in ceramic glazes, the presence of alkali metals and alkaline earth metals caused the loss of photocatalytic activity at the high temperature (≥1000 ℃).

It has been discovered that ZnO, as a semiconductor material, possesses not only a low cost but also exhibits photocatalytic activity. Furthermore, ZnO demonstrates exceptional performance in terms of interfusion and thermal stability when is combined with ceramics [17]. Additionally, the reaction between ZnO and TiO_2 yields enhanced photocatalytic effects compared to pure ZnO or pure TiO_2. Gonçalves [18] provided a comprehensive overview of the synthesis methods for ZnO and TiO_2, revealing the occurrence of three distinct phases, namely ilmenite rhombohedral $ZnTiO_3$, cubic spinel Zn_2TiO_4, and defective cubic $Zn_2Ti_3O_8$, which underwent transformation at different temperature ranges. Gabal [19] reported that Zn_2TiO_4 exhibited stability up to 1418 ℃, while Sandra investigated the impact of ZnO doping on the photocatalytic performance of Zn_2TiO_4, revealing that ZnO/Zn_2TiO_4 demonstrates superior photocatalytic properties compared to pure Zn_2TiO_4 [20].

The sol-gel hydrothermal method has been widely recognized for its ability to produce materials with enhanced photocatalytic performance. Cheng et al. [21] synthesized Fe/N codoped TiO_2 catalysts using sol-gel hydrothermal method, which exhibited excellent visible light photocatalytic degradation performance. This is attributed to the high surface area and optimal crystalline structure of the synthesized particles, which are key factors in improving photocatalytic efficiency. Besides, the method enables the production of materials at relatively low temperatures compared to traditional solid-state reactions. This not only saves energy but also helps in preserving the structural integrity of the materials, which is essential for maintaining high photocatalytic performance.

In this study, the ZnO-Zn_2TiO_4 composite was synthesized via a sol-hydrothermal method and incorporated into the conventional ceramic glaze, followed by sintering at 1300 ℃. Through comprehensive analysis of crystal phase composition, microstructure, and photocatalytic properties of the resulting ceramic glaze, this study presents a novel approach for fabricating high-temperature (1300 ℃)

ceramic glaze with enhanced photocatalytic activity. Furthermore, it could offer valuable technical support for imparting antibacterial and self-cleaning functionalities to traditional ceramics glazes.

2. Materials and methods

2.1. Synthesis of Zn-Ti-O compound materials

The TiO_2 sol was prepared as follows: 20 mL of CH_3CH_2OH (analytical grade, Jiangsu Qiangsheng Functional Chemical Corporation), 10 mL of $C_6H_{15}NO_3$ (analytical grade, Tianjin Kemiou Chemical Reagent Corporation), and 34 mL of $C_{16}H_{36}O_4Ti$ (analytical grade, Tianjin Kemiou Chemical Reagent Corporation) were combined in a beaker and stirred for 1 h. Subsequently, 1 mL of deionized water and 9 mL of CH_3CH_2OH were added to the beaker while continuing stirring for 1 h. Following this step, $Zn(CH_3COO)_2{\cdot}2H_2O$ (analytical grade, Xilong Scientific Corporation) with varying titanium-zinc ratios (Ti:Zn = 1:2, 1:3, 1:4, 1:5, 1:6, 1:7, 1:8, 1:9, and 1:10) was introduced into the aforementioned beaker and stirred for an additional hour.

The beaker's contents were transferred into a reactor and subjected to heating at 140 ℃ for 12 h. Subsequently, the dried mixture was transferred to an alumina crucible and sintered at 1300 ℃ in a muffle furnace. After cooling the muffle furnace to room temperature, the mixture within the alumina crucible was milled and passed through a 150-mesh screen to obtain Zn-Ti-O compound materials. The preparation process was illustrated in Figure 1.

The temperature gradient of the muffle furnace was as follows: first, the temperature ramped up from room temperature to 600 ℃ at a rate of 5 ℃/min and held steady at 600 ℃ for 0.5 h; second, the temperature increased from 600 to 1200 ℃ at the rate of 5 ℃/min and maintained 1200 ℃ for 0.5 h; third, the temperature rose from 1200 to 1300 ℃ at a rate of 5 ℃/min and maintained 1300 ℃ for 1 h; finally, the furnace cooled naturally back down to room temperature.

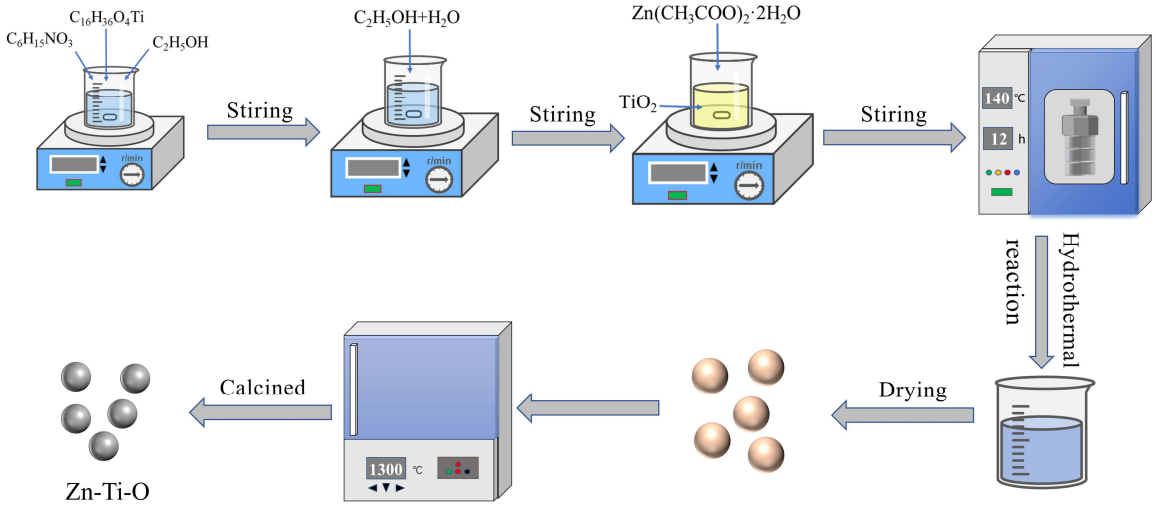

Figure 1. Schematic diagram of the preparation process of Zn-Ti-O compound materials.

2.2. Synthesis of the photocatalytic ceramic glaze

The Zn-Ti-O compound materials exhibiting the highest photocatalytic degradation performance toward methylene blue (MB) were selected for further study. The optimal Zn-Ti-O composite material (Ti:Zn = 1:8) with a mass percentage ranging from 5% to 25% was added to 300-mesh glaze powder, mixed thoroughly, and a 2 g mixture was prepared. This mixture was then placed into a mold with a diameter of 10 mm and a height of 10 mm, and pressed into a cylindrical shape. Then, the cylinder was placed on a ceramic body (diameter 25 mm) and burned in a muffle furnace at 1300 ℃. The composition of the ceramic glaze utilized in this study is presented in Table 1.

Table 1. The composition of ceramic glaze.

Composition	SiO_2	Al_2O_3	Na_2O	K_2O	MgO	CaO	Fe_2O_3	BaO
Content (wt%)	76.63	13.55	1.10	2.78	1.72	1.95	1.05	1.22

2.3. Characterization of the materials

The absorbance of MB following the photocatalytic reaction was measured using a UV-Vis spectrophotometer (UV-7600, Shanghai Jinghua Science and Technology Instrument Corporation).

The absorbance of the solid photocatalyst was measured using an Ultraviolet-visible spectrophotometer (UV-Vis, Shimadzu, UV-2600). The light absorption threshold of the sample was determined through tangential analysis within a scanning wavelength range of 200–800 nm.

The crystal structure of the samples was analyzed using an X-ray diffractometer (XRD, Ultima IV), with a scanning range of 2θ from 20 to 80°and a scanning speed of 10 °/min.

The Fourier infrared spectrometer (FT-IR, Shimadzu, IRTracer-100) was employed to assess the alterations in chemical bonds within the wavelength range of 400–2000 cm^{-1}.

The surface morphology and chemical composition of the samples were examined using scanning electron microscopy (SEM, Apreo S) and energy dispersive X-ray spectroscopy (EDX, EDAX ELECT PLUS). Additionally, the microstructure and lattice fringe of the samples were observed using a transmission electron microscope (TEM, JEM-2100).

2.4. Photocatalytic study

MB was used as the target pollutant to systematically evaluate the photocatalytic activity of the prepared samples. The experimental process is shown in Figure 2: (a) 0.6 g of Zn-Ti-O composite material was dispersed in 60 mL of MB solution with an initial concentration of 12 mg/L. Under room natural sunlight at 30 ± 2 ℃, 10 mL of MB solution was extracted every 24 h. The supernatant was obtained by centrifugation for absorbance detection. (b) Ceramic glaze slices with added Zn-Ti-O composite material were placed in 60 mL of MB solution with an initial concentration of 12 mg/L. Photocatalytic degradation experiments were carried out using natural light as the light source. Every 24 h, 10 mL of MB solution was extracted. The supernatant was obtained by centrifugation for absorbance detection. The degradation efficiencies of MB were calculated using Eq 1:

$$\text{Degradation} = (C_0 - C)/C_0 \times 100\% \quad (1)$$

where C_0 and C were the initial absorbance and degraded absorbance of the MB at 664 nm, respectively [22]. The photo-catalyst band gap energy (Eg) for the samples were measured using Eq 2:

$$E_g = 1240/\lambda g \quad (2)$$

where λg is the wavelength at the overlap of the vertical and horizontal portions in the ultraviolet-visible spectrophotometer with the tangential method [22].

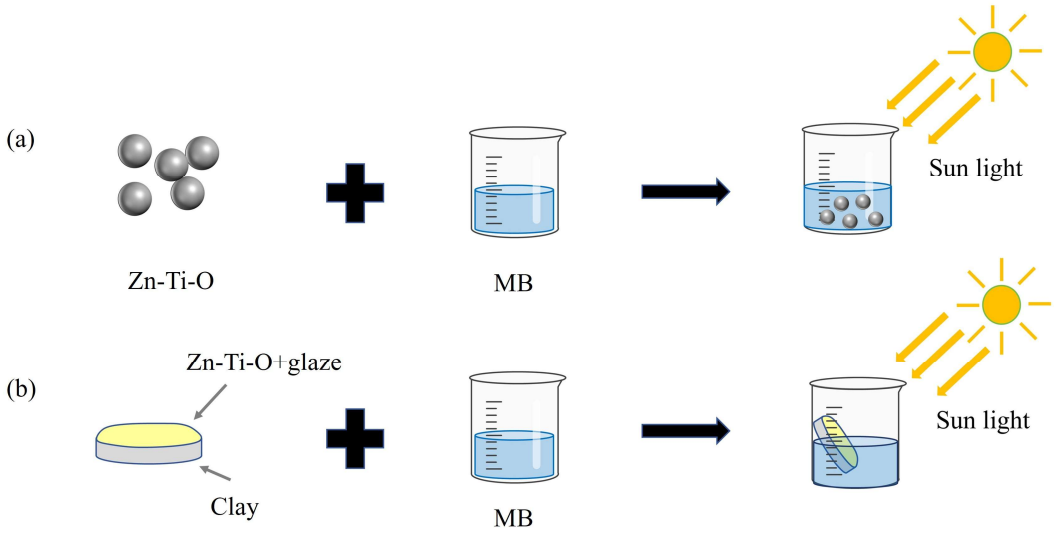

Figure 2. Schematic diagram of the photocatalytic experiment.

3. Results

3.1. Photocatalytic performance analysis of the Zn-Ti-O compound materials

The degradation of MB in the presence of Zn-Ti-O compound materials (with Ti:Zn molar ratios ranging from 1:2 to 1:10) are illustrated in Figure 3. For comparison, pure MB samples were tested under dark conditions (referred to as D) and sunlight exposure (referred to as L). As depicted in Figure 3a for the first day and Figure 3b for seven days, a gradual degradation of MB was observed with increasing reaction time. Notably, the degradation efficiency of MB was significantly enhanced when using Zn-Ti-O compound materials with a molar ratio of Ti:Zn between 1:5 and 1:8.

Figure 4 shows the degradation curve of MB by Zn-Ti-O composite materials (with Ti: Zn molar ratios ranging from 1:2 to 1:10) under natural light irradiation. As the irradiation time increased, the removal rate of all samples steadily increased. The self-degradation of MB under sunlight does impact the experimental results [23], but it did not mask the photocatalytic ability of ZnO-Zn_2TiO_4 for MB under ultraviolet light in our research. The Zn-Ti-O composite material with a Ti:Zn molar ratio of 1:8 exhibited excellent photocatalytic activity, with a removal rate of 96% after seven days of natural light irradiation, demonstrating outstanding photoresponsive ability.

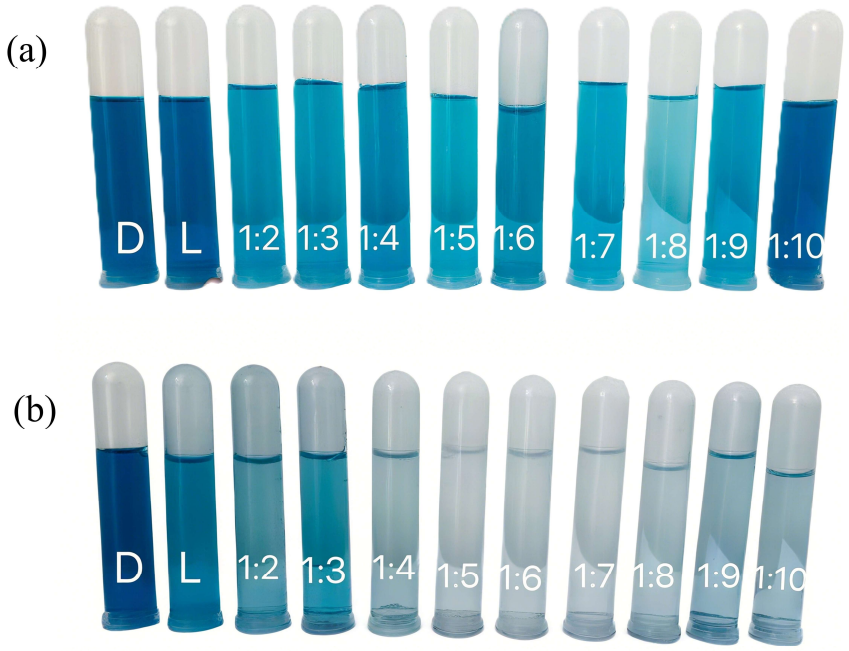

Figure 3. The pictures of degradation MB (a: 1 day, b: 7 days), MB-dark (named D), MB-sunlight (named L), and Zn-Ti-O compound materials (Ti:Zn = 1:2–1:10) reacted with MB under sunlight.

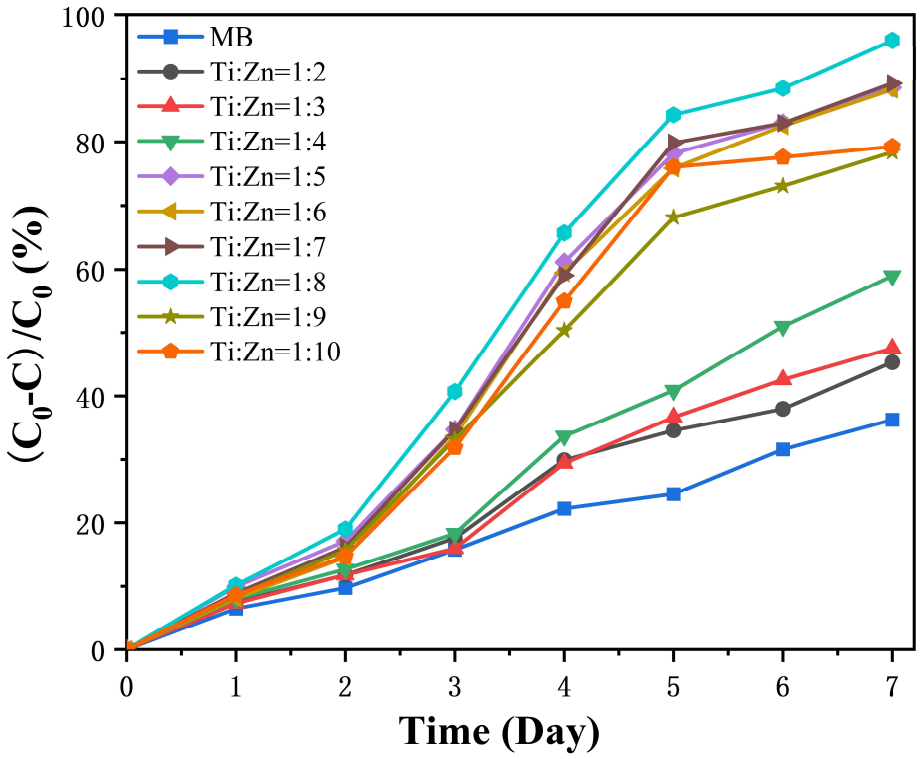

Figure 4. The degradation curves of MB solution by Zn-Ti-O compound materials (Ti:Zn = 1:2–1:10).

3.2. XRD analysis of the Zn-Ti-O compound material

The crystal structure of Zn-Ti-O compound materials (Ti:Zn = 1:8) was investigated by XRD, and the results are shown in Figure 5. The XRD patterns presented the diffraction peaks of two crystal phases: Zn_2TiO_4 (PDF-25-1164) and ZnO (PDF-36-1451). The presence of the rutile (TiO_2) phase was not detected. The presence of ZnO in the compound material was confirmed, and a portion of Zn^{2+} ions reacted with Ti^{4+} to form a new phase of Zn_2TiO_4. The XRD analysis presented in Figure 5 exhibited excellent agreement with other studies [24–26]. The reaction process between TiO_2 sol and $(CH_3COO)_2Zn{\cdot}2H_2O$ could be described as Eq 3:

$$(CH_3COO)_2Zn \cdot 2H_2O + Ti(OH)_4 \xrightarrow{400\ ℃} ZnO - TiO_2 \xrightarrow{>945\ ℃} ZnO + Zn_2TiO_4 \quad (3)$$

The occurrence of this reaction could facilitate the formation of a junction between ZnO and Zn_2TiO_4, thereby promoting the efficient separation of photo-generated carriers and resulting in enhanced photocatalytic performance [27].

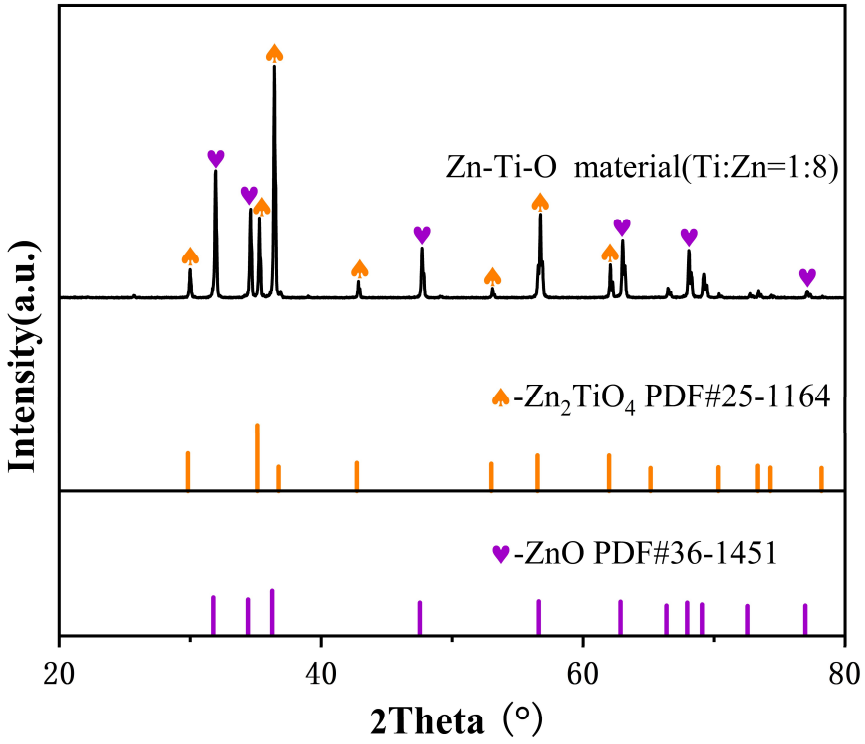

Figure 5. XRD pattern of the Zn-Ti-O compound material (Ti:Zn = 1:8).

3.3. Photocatalytic analysis of the ceramic glaze reacted with ZnO-Zn_2TiO_4

The ceramic glazes reacted with the superior photocatalytic compound material of ZnO-Zn_2TiO_4 (Ti:Zn = 1:8) at mass percentages ranging from 5% to 25%, followed by sintering at a temperature of 1300 ℃. The photocatalytic performance of the ceramic glazes was evaluated by reacting with MB under sunlight conditions. For comparison, MB samples were tested in the dark (referred to as D-MB) and under sunlight (referred to as L-MB). It was observed that the absorbance of all collected MB

samples gradually decreased over a period of 21 days, but the ceramic glazes reacted with ZnO-Zn_2TiO_4 exhibited superior performance in degrading MB. To identify the best catalytic performance among the ceramic glazes, an enlarged picture showing the degradation of MB over a span of 21 days is presented in Figure 6. After 21 days, almost complete degradation of MB was achieved using the ceramic glaze containing a mass percentage of ZnO-Zn_2TiO_4 at 15%, resulting in a degradation rate of MB reaching up to 96.13%.

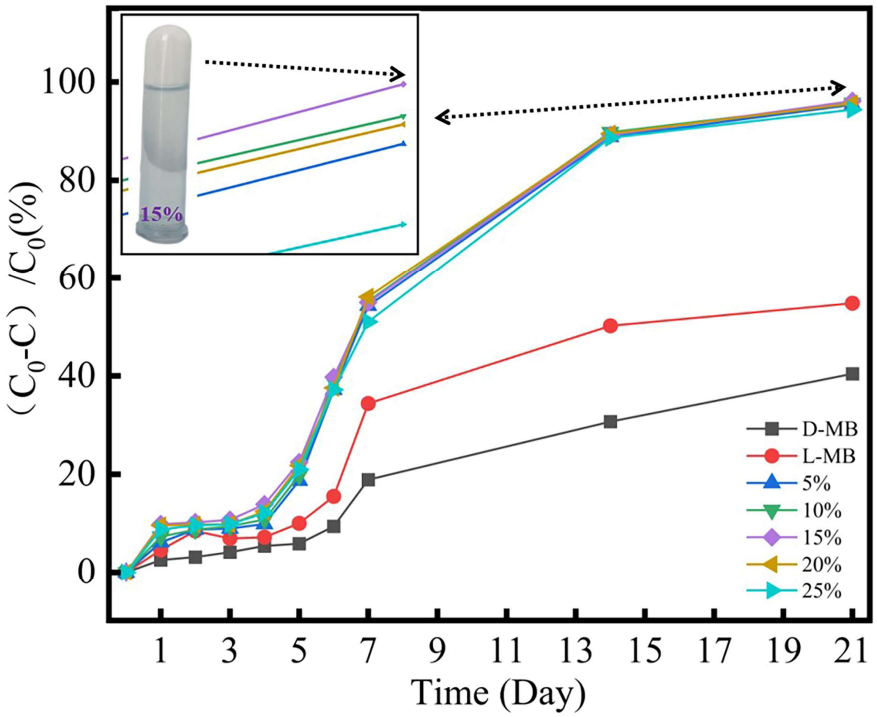

Figure 6. The UV-Vis spectrum absorbance of MB degraded by different materials during the 21 days.

3.4. XRD analysis of ceramic glaze

The major crystalline phases of the ceramic glaze consisted of SiO_2 (PDF-46-1045), Al_2O_3 (PDF-04-0878), and $KAlSi_3O_8$ (PDF-19-0926) in Figure 7a, which were consistent with the composition of the ceramic glaze as shown in Table 1. However, as depicted in Figure 7b, when the ceramic glaze reacted with ZnO-Zn_2TiO_4 at a mass percentage of 15%, new crystalline phases, including $Zn_4Al_{22}O_{37}$ (PDF-23-1491), ZnO (PDF-36-1451), and Zn_2TiO_4 (PDF-25-1164), appeared. Notably, there was a minor change observed: the crystalline phase $KAlSi_3O_8$ (2θ = 28.072°) disappeared, while a new crystalline phase $Zn_4Al_{22}O_{37}$ (PDF-23-1491) emerged instead. This phenomenon could be attributed to the stronger polarization ability of Zn^{2+} compared to Na^+, resulting in easier generation of $Zn_4Al_{22}O_{37}$ and transformation of NaO-SiO_2 into the ceramic glaze matrix. XRD analysis confirmed that after sintering at 1300 ℃, the composite photocatalyst consisting of ZnO-Zn_2TiO_4 was stably integrated into the ceramic glaze.

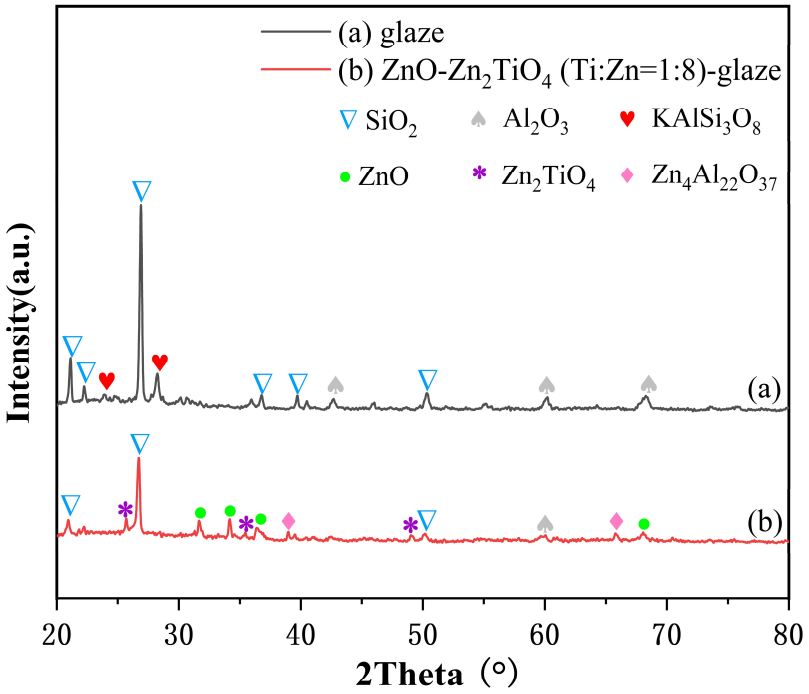

Figure 7. XRD analysis of the ceramic glazes. (a) The ceramic glaze and (b) the ceramic glaze reacted with 15% mass percentage ZnO-Zn_2TiO_4(Ti:Zn = 1:8).

3.5. FT-IR analysis of ceramic glaze

To further analyze the reaction between the ceramic glaze and ZnO-Zn_2TiO_4, Figure 8 presents the FT-IR analysis of different materials. In Figure 8a, for the ceramic glaze sintered at 1300 ℃, an absorption peak at 806 cm^{-1} was observed, which could be attributed to the asymmetric stretching vibration of Si–O(Si) and Si–O(Al) bridge bonds. Additionally, a peak at 421 cm^{-1} was identified as bending vibrations of O–Si–O and O–Al–O bonds. The presence of these two absorption peaks was consistent with the composition of the ceramic glaze [28].

The FT-IR pattern of ZnO-Zn_2TiO_4 in Figure 8b revealed that the absorption peak at 623 cm^{-1} could be attributed to the absorption band of [TiO_6] octahedral groups, while the absorption peaks at 468 and 399 cm^{-1} were associated with the absorption bands of [ZnO_4] tetrahedral groups. Upon reaction with ceramic glaze containing 15 wt% mass percentage of ZnO-Zn_2TiO_4, as shown in Figure 8c, a new absorption peak emerged at 659 cm^{-1}, which was assigned to the absorption band of [TiO_6] octahedral groups, along with additional peaks observed at 498 and 412 cm^{-1} corresponding to the absorption bands of [ZnO_4] tetrahedral groups [29,30].

The absorption band exhibited a higher wave number and weaker intensity compared to the corresponding materials in Figure 8b. Furthermore, the absorption peak at 799 cm^{-1}, associated with asymmetric stretching vibration of Si–O(Si) and Si–O(Al) bridge bonds, shifted to a lower wave number and displayed weaker intensity than that observed in the ceramic glaze shown in Figure 8a. The changes depicted in Figure 8c, as opposed to the ceramic glaze, could be attributed to the fusion of Zn^{2+} within the ceramic glaze at high temperatures, resulting in fracture of Si–O(Al) bridge bonds [27]. The FT-IR analysis was consistent with XRD analysis (Figure 7).

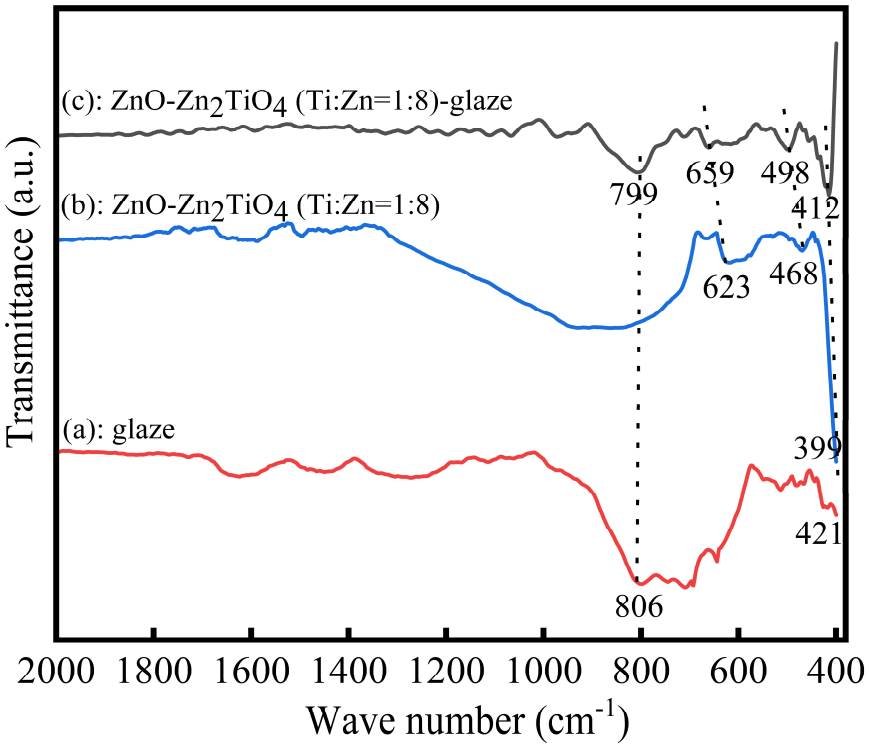

Figure 8. FT-IR analysis of ceramic glazes. (a) Glaze, (b) $ZnO\text{-}Zn_2TiO_4$ (Ti:Zn = 1:8), and (c) ceramic glaze mixed with 15% mass percentage $ZnO\text{-}Zn_2TiO_4$ (Ti:Zn = 1:8).

3.6. SEM-EDS analysis of ceramic glaze

The grain size of $ZnO\text{-}Zn_2TiO_4$, as observed in Figure 9a, ranged from 1 to 5 μm and exhibited various shapes, including triangles, hexagons, rectangles, and circles [31]. In Figure 9b, the microstructure of the ceramic glaze mixed with 15% mass percentage of $ZnO\text{-}Zn_2TiO_4$ was depicted, revealing that the triangles and hexagons of $ZnO\text{-}Zn_2TiO_4$ were present and well-integrated with the ceramic glaze. To further confirm the presence of $ZnO\text{-}Zn_2TiO_4$, EDS spectra analysis was conducted on the marked area containing triangles in Figure 9b. As shown in Figure 9c, elements such as C, Au, O, Ti, Zn, and Al were detected in the sample. The presence of C originated from the conductive tape, while Au was derived from the conductive coating. Notably, O, Ti, and Zn were attributed to $ZnO\text{-}Zn_2TiO_4$. The element Al was identified as originating from a crystalline phase known as $Zn_4Al_{22}O_{37}$. Furthermore, the results obtained through EDS analysis were consistent with those obtained through XRD analysis.

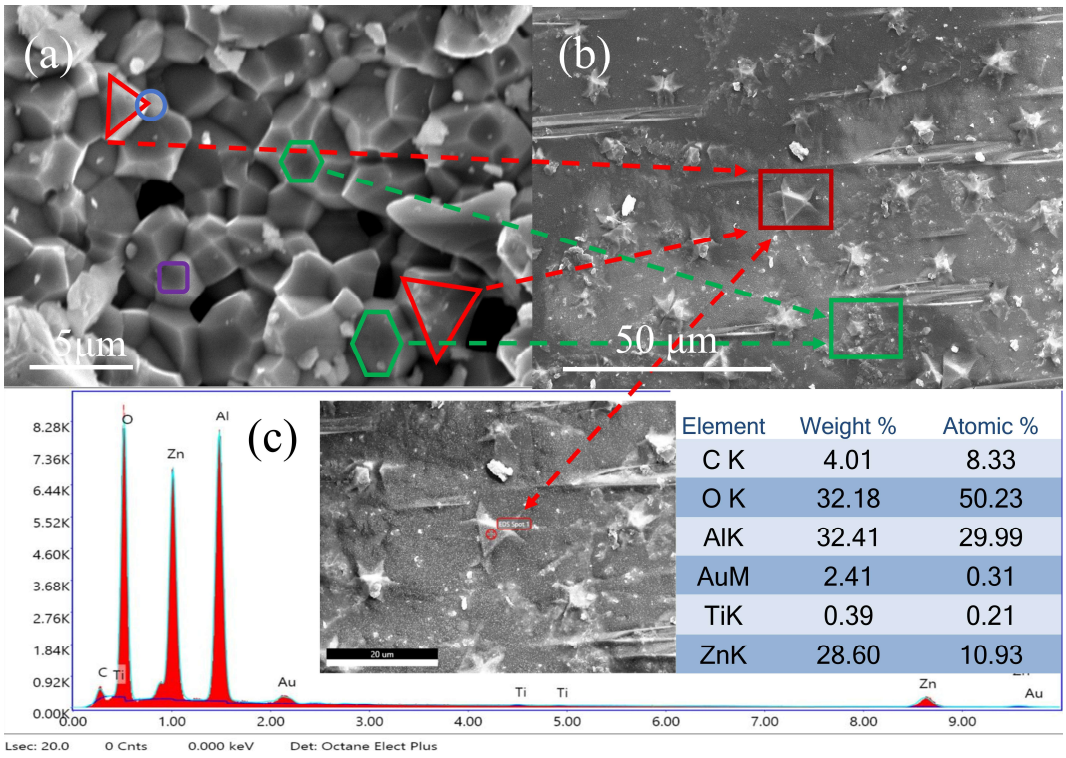

Figure 9. SEM-EDS analysis of ceramic glaze. (a) ZnO-Zn_2TiO_4(Ti:Zn = 1:8), (b) the ceramic glaze mixed with 15% mass percentage of ZnO-Zn_2TiO_4(Ti:Zn = 1:8), and (c) EDS spectra of the ZnO-Zn_2TiO_4 in the ceramic glaze.

3.7. TEM analysis of ceramic glaze

As depicted in Figure 10a, distinct lattice striations were observed in selected regions, with lattice fringes of 0.247 and 0.255 nm corresponding to the (101) crystal plane for ZnO (PDF-36-1451) and the (311) crystal plane for Zn_2TiO_4 (PDF-25-1164), respectively. The poly-crystalline structure of ZnO-Zn_2TiO_4 (Ti:Zn = 1:8) was confirmed, exhibiting excellent crystallinity after sintering at 1300 ℃. Analysis of Figure 10a revealed the formation of a heterojunction between ZnO and Zn_2TiO_4 at the interface region, which could enhance the efficiency of photogenerated electron-hole separation [27,32]. When the ceramic glaze was mixed with a mass percentage of 15% ZnO-Zn_2TiO_4 and sintered at 1300 ℃, as shown in Figure 10b, new poly-crystalline structures similar to the (311) plane for Zn_2TiO_4 (PDF-25-1164) in Figure 10c, the (101) plane for ZnO (PDF-36-1451) in Figure 10d, the (101) plane for SiO_2 (PDF-46-1045) in Figure 10e, and the (110) plane for $Zn_4Al_{22}O_{37}$ (PDF-23-1491) in Figure 10f, were observed in the ceramic glaze. The TEM analysis indicated that ZnO-Zn_2TiO_4 was a poly-crystalline structure and well fused with the ceramic glaze, which consistently supported the results of XRD and SEM analysis.

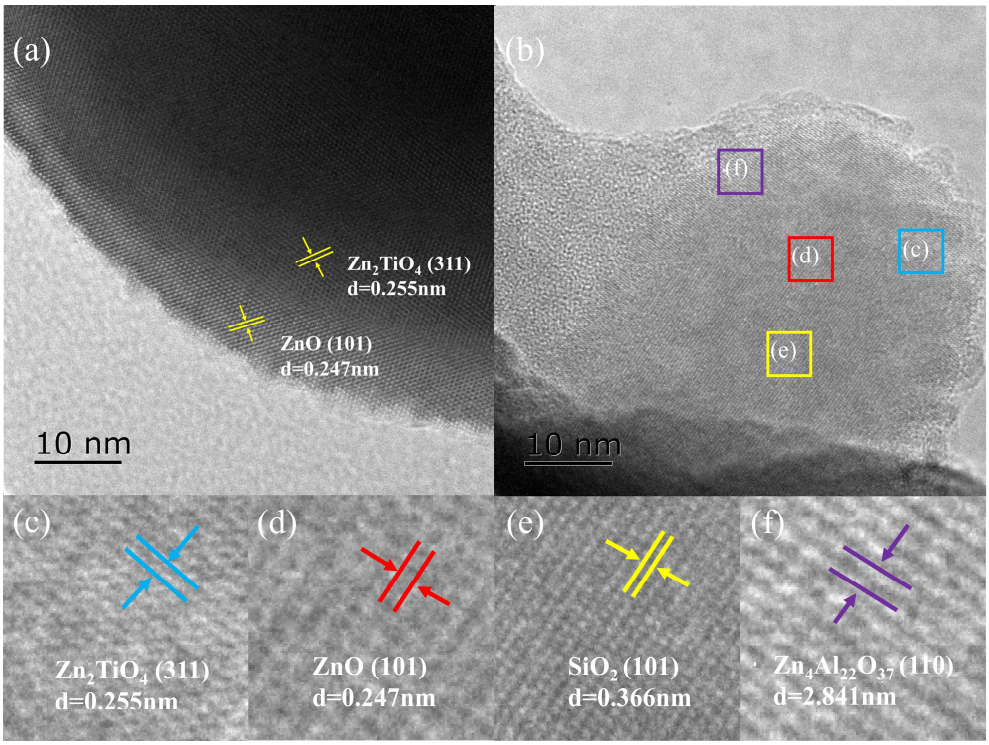

Figure 10. TEM analysis of the ceramic glaze. (a) ZnO-Zn_2TiO_4 (Ti:Zn = 1:8), (b) the ceramic glaze mixed with 15% mass percentage ZnO-Zn_2TiO_4 (Ti:Zn = 1:8), (c) lattice fringes of Zn_2TiO_4 (311) plane, (d) lattice fringes of ZnO (101) plane, (e) lattice fringes of SiO_2 (101) plane, and (f) lattice fringes of $Zn_4Al_{22}O_{37}$ (110) plane.

3.8. UV-Vis analysis and energy gap calculation of ceramic glaze

To investigate the impact of ZnO-Zn_2TiO_4 on the photocatalytic activity of the ceramic glaze, the UV-Vis spectrum analysis is presented in Figure 11. The UV-Vis absorption threshold value for the ceramic glaze in Figure 11a was determined to be 438 nm, corresponding to an energy gap calculation of 2.83eV. The UV-Vis absorption threshold value for ceramic glaze mixed with 15% mass percentage ZnO-Zn_2TiO_4 (Ti:Zn = 1:8) in Figure 11b was determined to be 456 nm, corresponding to an energy gap calculation of 2.72 eV. For ZnO-Zn_2TiO_4 in Figure 11c, the UV-Vis absorption threshold value was measured at 476 nm, resulting in an energy gap calculation of 2.61 eV.

Compared with the ceramic glaze, it was observed that when reacted with a mass percentage of 15% ZnO-Zn_2TiO_4, there was an increase in the UV-Vis absorption threshold from 438 to 456 nm (the energy gap has been reduced from 2.83 to 2.72eV). This demonstrated that by incorporating ZnO-Zn_2TiO_4 into the ceramic glaze, its photocatalytic performance could be effectively enhanced within the visible region.

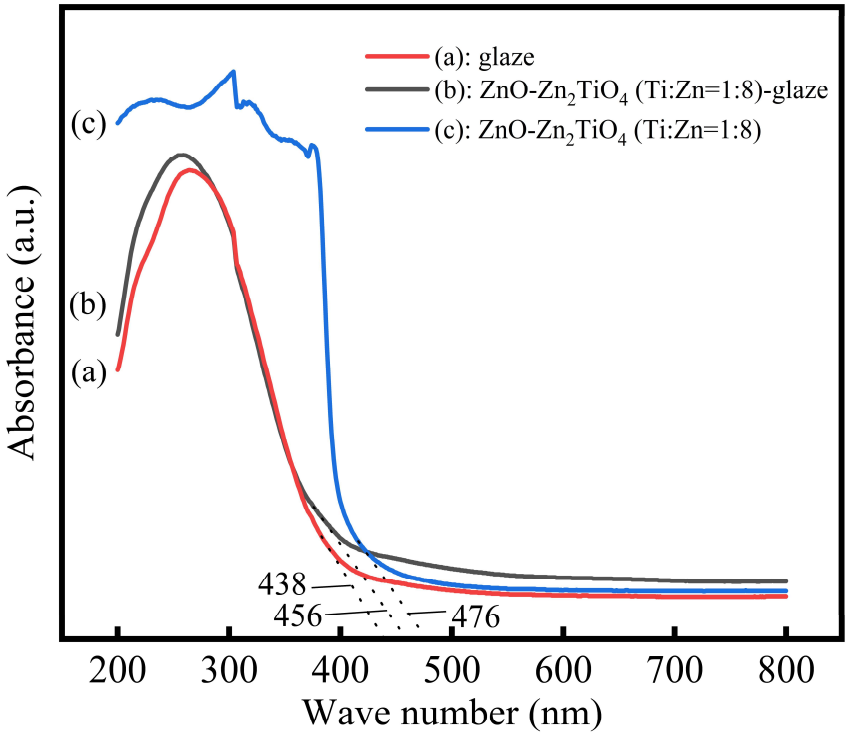

Figure 11. UV-Vis analysis: (a) ceramic glaze, (b) ceramic glaze mixed with 15% mass percentage ZnO-Zn_2TiO_4 (Ti:Zn = 1:8), and (c) ZnO-Zn_2TiO_4 (Ti:Zn = 1:8).

4. Conclusions

Our objective of this study was to assess the impact of ZnO-Zn_2TiO_4 on the photocatalytic properties of the ceramic glaze sintered at 1300 ℃. Photocatalytic evaluation results for MB decolorization revealed that the ceramic glaze incorporating 15% mass percentage of ZnO-Zn_2TiO_4 (with the Ti:Zn ratio of 1:8) exhibited superior photocatalytic efficiency compared to all other samples, achieving a degradation rate of 96.13% after 21 days under sunlight irradiation.

From the analysis of the XRD and the SEM-EDX, the ZnO-Zn_2TiO_4 exists as a poly-crystalline structure in the ceramic glaze sintered at 1300 ℃. According to the analysis of the FT-IR, the Zn^{2+} fused in the glaze at high temperature, causing the silicon-oxygen bond to break. As shown in the TEM, it could be found that the poly-crystalline of ZnO and Zn_2TiO_4 formed an interface region at the crystal plane. This intense interaction between the two could form a heterojunction, which could improve the efficiency of photogenerated electrons and holes separation.

The photo-catalyst band gap energy (Eg) of the ceramic glaze was measured in the UV-Visible spectrum, demonstrating a significant enhancement in photocatalytic performance after reaction with ZnO-Zn_2TiO_4 within the visible region. These findings presented a novel approach for fabricating high temperature ceramic glazes (1300 ℃) with exceptional photocatalytic properties and offer valuable technical support for the antibacterial and self-cleaning characteristics of ceramic glazes.

Use of AI tools declaration

The authors declare they have not used Artificial Intelligence (AI) tools in the creation of this article.

Acknowledgments

This work was supported and grants funded by Hunan Provincial Natural Science Foundation of China (2021JJ50036,2025JJ70041) and Ministry of Education Industry-university Cooperative Education Project of China (220904082254614), excellent youth funding of Hunan Provincial Education Department (24B0526).

Author contributions

Weida Hu: project leader, experimental plan formulation, funding acquisition, supervision; Jiaming Lin: writing-original draft, editing, data collection analysis and interpretation of results; Qi Xu: writing-original draft, experimental setup, experimentation; Tong Yu: experimental testing and data collection.

Conflict of interest

The authors declare no conflict of interest.

References

1. Murugan K, Subasri R, Rao TN, et al. (2013) Synthesis, characterization and demonstration of self-cleaning TiO_2 coatings on glass and glazed ceramic tiles. *Prog Org Coat* 76: 1756–1760. https://doi.org/10.1016/j.porgcoat.2013.05.012
2. Hofer M, Penner D (2011) Thermally stable and photocatalytically active titania for ceramic surfaces. *J Eur Ceram Soc* 31: 2887–2896. https://doi.org/10.1016/j.jeurceramsoc.2011.07.016
3. Monrós G, Liusar M, Badenes J, et al. (2022) Sol-gel ceramic glazes with photocatalytic activity. *J Sol-Gel Sci Techn* 02: 535–549. https://doi.org/10.1007/s10971-022-05787-z
4. Liu J, Wang Y, Ma J, et al. (2019) A review on bidirectional analogies between the photocatalysis and antibacterial properties of ZnO. *J Alloy Compd* 783: 898–918. https://doi.org/10.1016/j.jallcom.2018.12.330
5. Leong S, Razmjou A, Wang K, et al. (2014) TiO_2 based photocatalytic membranes: A review. *J Membrane Sci* 472: 167–184. https://doi.org/10.1016/j.memsci.2014.08.016
6. Yu Z, Qiu R, Li H, et al. (2016) Preparation and photocatalytic activity of SnO_2. *Mater Lett* 170: 25–30. https://doi.org/10.1016/j.matlet.2015.12.100
7. Wang Q, Zhang W, Hu X, et al. (2021) Hollow spherical WO_3/TiO_2 heterojunction for enhancing photocatalytic performance in visible-light. *J Water Process Eng* 40: 101943. https://doi.org/10.1016/j.jwpe.2021.101943
8. Qin R, Meng F, Khan MW, et al. (2019) Fabrication and enhanced photocatalytic property of TiO_2-ZnO composite photocatalysts. *Mater Lett* 240: 84–87. https://doi.org/10.1016/j.matlet.2018.12.139
9. Hamdi A, Ferreira DP, Ferraria AM, et al. (2016) TiO_2-CdS nanocomposites: Effect of CdS oxidation on the photocatalytic activity. *J Nanomater* 2016: 6581691. https://doi.org/10.1155/2016/6581691

10. Sangchay W (2016) The self-cleaning and photocatalytic properties of TiO_2 doped with SnO_2 thin films preparation by sol-gel method. *Energy Procedia* 89: 170–176. https://doi.org/10.1016/j.egypro.2016.05.023
11. Machida M, Norimoto K, Kimura T (2005) Antibacterial activity of photocatalytic titanium dioxide thin films with photodeposited silver on the surface of sanitary ware. *J Am Ceram Soc* 88: 95–100. https://doi.org/10.1111/j.1551-2916.2004.00006.x
12. Määttä J, Piispanen M, Kuisma R, et al. (2007) Effect of coating on cleanability of glazed surfaces. *J Eur Ceram Soc* 27: 4555–4560. https://doi.org/10.1016/j.jeurceramsoc.2007.02.204
13. Cacciotti I, Nanni F, Campaniello V, et al. (2014) Development of a transparent hydrorepellent modified SiO_2 coatings for glazed sanitarywares. *Mater Chem Phys* 146: 240–252. https://doi.org/10.1016/j.matchemphys.2014.03.005
14. Zhuang J, Liu P, Dai W, et al. (2010) A novel application of nano anticontamination technology for outdoor high-voltage ceramic insulators. *Int J Appl Ceram Tec* 7: 46–53. https://doi.org/10.1111/j.1744-7402.2009.02395.x
15. Zeng Z, Cheng P, Hong Y, et al. (2010) Fabrication of a photocatalytic ceramic by doping Si-, P-, and Zr- modified TiO_2 nanopowders in glaze. *J Am Ceram Soc* 93: 2948–2951. https://doi.org/10.1111/j.1551-2916.2010.03910.x
16. He C, Tian B, Zhang J (2010) Thermally stable SiO_2-doped mesoporous anatase TiO_2 with large surface area and excellent photocatalytic activity. *J Colloid Interf Sci* 344: 382–389. https://doi.org/10.1016/j.jcis.2010.01.002
17. Tulyaganov DU, Agathopoulos S, Fernandes HR, et al. (2007) The influence of incorporation of ZnO-containing glazes on the properties of hard porcelains. *J Eur Ceram Soc* 27: 1665–1670. https://doi.org/10.1016/j.jeurceramsoc.2006.05.011
18. Gonçalves RA, Toledo RP, Joshi N, et al. (2021) Green synthesis and applications of ZnO and TiO_2 nanostructures. *Molecules* 26: 2236. https://doi.org/10.3390/molecules26082236
19. Gabal MA, Angari YMAl (2022) Zinc titanates nanopowders: Synthesis and characterization. *Mater Res Express* 9: 025010. https://doi.org/10.1088/2053-1591/ac5709
20. Mayén-Hernández SA, Torres-Delgado G, Castanedo-Pérez R, et al. (2007) Photocatalytic activity in Zn_2TiO_4 + ZnO thin films obtained by the sol-gel process. *J Adv Oxid Technol* 10: 90–93. https://doi.org/10.1515/jaots-2007-0115
21. Cheng HH, Chen SS, Yang SY, et al. (2018) Sol-gel hydrothermal synthesis and visible light photocatalytic degradation performance of Fe/N codoped TiO_2 catalysts. *Materials* 11: 939. https://doi.org/10.3390/ma11060939
22. Yang T, Liu Y, Xia G, et al. (2021) Degradation of formaldehyde and methylene blue using wood-templated biomimetic TiO_2. *J Clean Prod* 329: 129726. https://doi.org/10.1016/j.jclepro.2021.129726
23. Paredes P, Rauwel E, Wragg D, et al. (2023) Sunlight-driven photocatalytic degradation of methylene blue with facile one-step synthesized Cu-Cu_2O-Cu_3N nanoparticle mixtures. *Nanomaterials* 138: 1311. https://doi.org/10.3390/nano13081311
24. Sun X, Wang S, Shen C, et al. (2016) Efficient photocatalytic hydrogen production over Rh-doped inverse spinel Zn_2TiO_4. *ChemCatChem* 813: 2289–2295. https://doi.org/10.1002/cctc.201600425
25. Siriwong C, Phanichphant S (2011) Flame-made single phase Zn_2TiO_4 nanoparticles. *Mater Lett* 65: 2007–2009. https://doi.org/10.1016/j.matlet.2011.03.058

26. Chai Y, Li L, Lu J, et al. (2019) Germanium-substituted Zn_2TiO_4 solid solution photocatalyst for conversion of CO_2 into fuels. *J Catal* 371: 144–152. https://doi.org/10.1016/j.jcat.2019.01.017
27. Arin J, Thongtem S, Phuruangrat A, et al. (2017) Characterization of ZnO-TiO_2 and zinc titanate nanoparticles synthesized by hydrothermal process. *Res Chem Intermediat* 43: 3183–3195. https://doi.org/10.1007/s11164-016-2818-y
28. Leśniak M, Partyka J, Sitarz M (2016) Impact of ZnO on the structure of aluminosilicate glazes. *J Mol Struct* 1126: 251–258. https://doi.org/10.1016/j.molstruc.2016.01.009
29. Chaves AC, Lima SJG, Araújo RCMU, et al. (2006) Photoluminescence in disordered Zn_2TiO_4. *Int J Quantum Chem* 179: 985–992. https://doi.org/10.1016/j.jssc.2005.12.018
30. Mebrek A, Alleg S, Benayache S, et al. (2018) Preparation and characterization of spinel type Zn_2TiO_4 nanocomposite. *Ceram Int* 44: 10921–10928. https://doi.org/10.1016/j.ceramint.2018.03.153
31. Manchala S, Nagappagari LR, Venkatakrishnan SM, et al. (2018) Facile synthesis of noble-metal free polygonal Zn_2TiO_4 nanostructures for highly efficient photocatalytic hydrogen evolution under solar light irradiation. *Int J Hydrogen Energ* 43: 13145–13157. https://doi.org/10.1016/j.ijhydene.2018.05.035
32. Janani FZ, Khiar H, Taoufik N, et al. (2023) ZnO-Zn_2TiO_4 heterostructure for highly efficient photocatalytic degradation of pharmaceuticals. *Environ Sci Pollut R* 30: 81403–81416. https://doi.org/10.1007/s11356-022-22791-6

AIMS Press